in silico Plants, 2023, **5**, 1–12
https://doi.org/10.1093/insilicoplants/diad012
Advance access publication 14 September 2023
Original Research

Original Research

Phloem anatomy restricts root system architecture development: theoretical clues from *in silico* experiments

Xiao-Ran Zhou, Andrea Schnepf, Jan Vanderborght, Daniel Leitner, Harry Vereecken and Guillaume Lobet*

Institute of Bio- and Geosciences, Agrosphere (IBG-3), Forschungszentrum Jülich GmbH, Wilhelm-Johnen-Straße, 52428 Jülich, Germany

*Corresponding author's e-mail address: g.lobet@fz-juelich.de

Handling Editor: Xin-Guang Zhu

ABSTRACT

Plant growth and development involve the integration of numerous processes, influenced by both endogenous and exogenous factors. At any given time during a plant's life cycle, the plant architecture is a readout of this continuous integration. However, untangling the individual factors and processes involved in the plant development and quantifying their influence on the plant developmental process is experimentally challenging. Here we used a combination of computational plant models (CPlantBox and PiafMunch) to help understand experimental findings about how local phloem anatomical features influence the root system architecture. Our hypothesis was that strong local phloem resistance would restrict local carbon flow and locally modify root growth patterns. To test this hypothesis, we simulated the mutual interplay between the root system architecture development and the carbohydrate distribution to provide a plausible mechanistic explanation for several experimental results. Our *in silico* experiments highlighted the strong influence of local phloem hydraulics on the root growth rates, growth duration and final length. The model result showed that a higher phloem resistivity leads to shorter roots due to the reduced flow of carbon within the root system. This effect was due to local properties of individual roots, and not linked to any of the pleiotropic effects at the root system level. Our results open a door to a better representation of growth processes in a plant computational model.

KEYWORDS: Carbon; modeling; phloem; structure; vasculature; water.

1. INTRODUCTION

Plants develop complex architectures, both above ground (the shoot) and below ground (the root system) (Drouet and Pagès 2003). An optimal architecture ensures that the different plant organs are ideally positioned in the environment to capture resources needed for their growth (Pagès *et al.* 2014; Kahlen and Chen 2015). Belowground, an efficient root system architecture ensures that individual roots are able to take up water and nutrients from the soil and transport them to the shoot (De Bauw *et al.* 2020). Since the availability of soil resources is highly heterogeneous, both in space and time, plants need to constantly adapt and develop their root system architecture (Morandage *et al.* 2021). Understanding how this development is controlled and regulated by the plant is an important open question.

The development of the root system fundamentally relies on three simple processes: root growth, self-re-orientation within the soil matrix (tropism) and production of next order (generation) of roots (Leitner *et al.* 2010). These new branches, or laterals, develop further following the same dynamical mechanisms. However, despite being individually simple, the assembly of these processes at the plant level quickly becomes complex as growth, tropism and branching are all influenced by exogenous and endogenous factors (Sharp *et al.* 2004; Ahmed *et al.* 2022). Exogenously, for instance, local soil water gradients can have a large influence on all the three processes (growth, tropism and branching). Endogenously, the amount of carbohydrates reaching individual root tips can restrict their growth. The amount of carbon reaching each growing tip is then directly linked to the growth potential and development of the root system.

Unlike leaves, roots are non-photosynthetic organs. The respiration maintenance (carbon consumed to maintain the living organ) and growth at each location of a root system relies on the

carbon that is transported from the leaves. This long-distance transportation from leaves to root takes place within the phloem vasculature, which is continuous throughout the whole plant. According to the pressure-flow model of phloem transport, several key factors influence carbohydrates transport within the plant:

1. the loading rate of carbohydrates into the phloem sieve tubes in source organs (e.g. leaves) (de Vries *et al.* 2021),
2. the unloading rate of carbohydrates out of the phloem sieve tubes in sink organs (e.g. roots) (Uys *et al.* 2021),
3. the connections between the different plant organs (Delory *et al.* 2016) and
4. the distribution of resistances of individual phloem vessels throughout the plant (Knoblauch *et al.* 2016).

How carbon transport controls growth is therefore a complex, multi-scale problem. Locally, the root phloem resistivity is influenced by its anatomy (e.g. the radius of the sieve tubes as shown in Supporting Information—Fig. S1); holistically, the length of a root changes its total resistance and influences the amount of available carbon at its tip (Fig. 1). The growth of a plant is therefore influenced by its architecture and anatomy, and defines both at the same time. This creates a complex feedback loop between the phloem flow and the development of the root system (see Supporting Information—Figs. S3 and S4). Complex patterns, which are independent of potential pleiotropic effects, can be caused by local anatomical variations. From an experimental point of view, disentangling the different processes (e.g. how resistivity of sieve tubes affects root growth rate and final length) to understand their relative contribution is a complex task (Bidel *et al.* 2000; Dilkes *et al.* 2004). From a simulation point of view, we previously presented a model of carbon and flow within a whole plant structure (Zhou *et al.* 2020), but without feedback loops between the carbon allocation and local growth. In this context, a feedback loop between anatomical structures (phloem and xylem) and architecture was not complete.

Here we present an *in silico* analysis of such a complex system and further use the outcome to explain experimental observations. To do so, we deepened the coupling between a computational model of plant growth and development, CPlantBox (Zhou *et al.* 2020), and a solver of the pressure-flow model of carbohydrates movement within the plant structure, PiafMunch (Lacointe and Minchin 2008, 2019). Compared to the previous publication (Zhou *et al.* 2020), which only transfers information from CPlantBox to PiafMunch, the coupling in this publication also transfers information from PiafMunch to CPlantBox

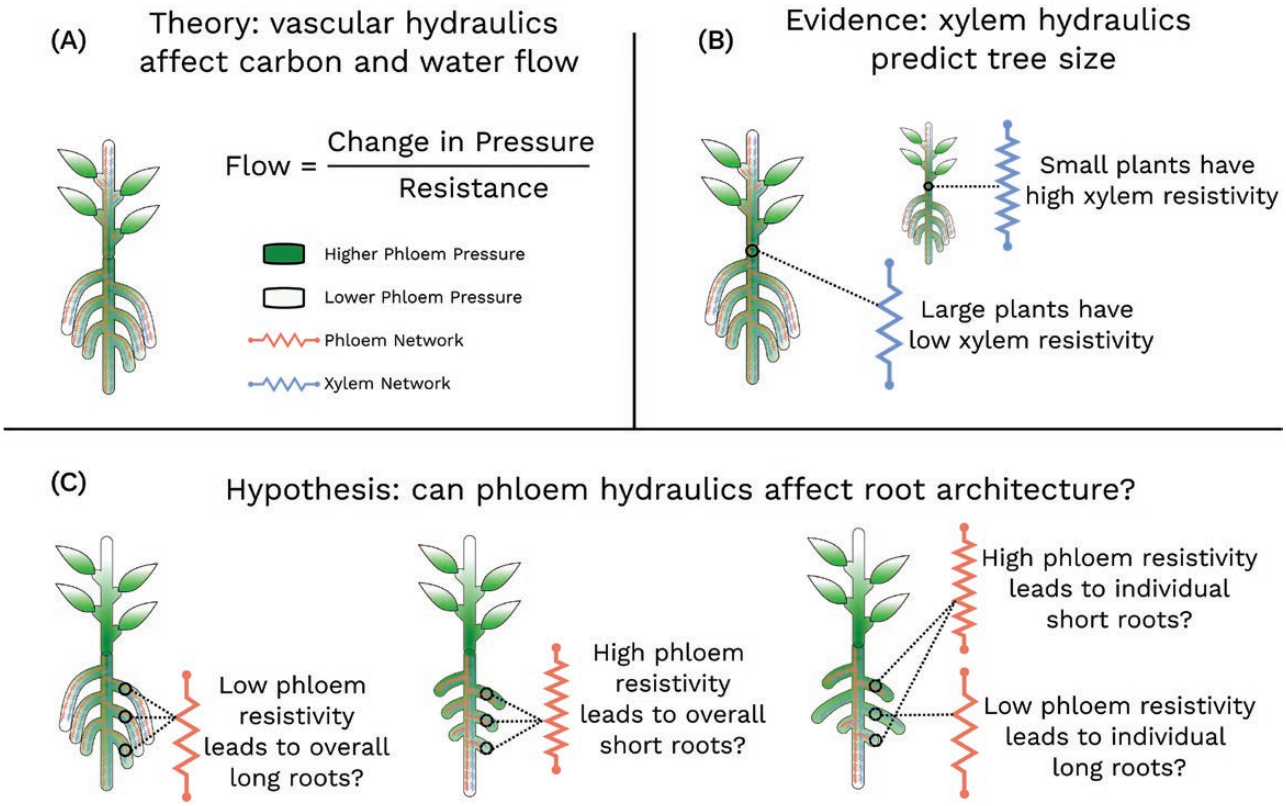

Figure 1. Plant vasculature can cast the shape of architecture. A: The carbon and water flow reaching the end of the organ part is calculated through pressure and resistance. Thus, the phloem resistance affects the carbon flow at root tips. B: Previous experimental studies have shown that xylem hydraulics affect plant size (Zhong *et al.* 2019; García-Cervigón *et al.* 2020). C: We hypothesize that local phloem restrictions (high resistivity) influence local growth patterns and ultimately root system architecture. For example, low phloem resistivities result in long roots in the left plant; high phloem resistivity result in shorter roots in the middle plant; mixed low and high phloem resistivity result in mixed lateral root length in the right plant. The effect of resistivity on root length can be independent of potential pleiotropic effects .

Table 1. Comparison of the sensitivity in the *in silico* experiments (1–3).

	Taproot	Lateral root	
	Single sieve-tube resistivity	**Single sieve-tube resistivity**	**Mixed lateral roots**
In silico experiment 1	Varied	Fixed	No
In silico experiment 2	Fixed	Varied	No
In silico experiment 3	Fixed	Varied	Yes

(carbon availability). Using this improved model coupling, we designed three *in silico* experiments (Table 1) *to* show how carbohydrates transport and root system development are influencing each other and how they are influenced by local root phloem properties.

Our main hypothesis is that local phloem hydraulic properties can shape the root growth and development, and therefore modify the root system architecture as a whole. More specifically, during *in silico* experiment 1, we tested how changes in *taproot* resistivity influences the root architecture. During *in silico* experiment 2, we tested how the root architecture is influenced by homogeneous changes in *lateral* resistivity. Finally, *in silico* experiment 3, we randomly changed local lateral root resistivity to isolate potential pleiotropic effects of changes in carbon allocation.

2. MATERIAL AND METHODS

2.1 Brief descriptions of the models CPlantBox and PiafMunch

CPlantBox is a generic computational plant model (Zhou *et al.* 2020) and it was designed to create a growing plant structure containing both the root and the shoot based on growth rules that describe organ elongation, branching, orientation and senescence. CPlantBox can be connected to other models, in such a way that the simulated architecture can be used as a numerical grid to simulate diverse functions such as water flow (Lobet *et al.* 2014; Morandage *et al.* 2021), exudation (Landl *et al.* 2021), nutrient uptake (De Bauw *et al.* 2020) or carbon and water flow (Zhou *et al.* 2020).

PiafMuch (Lacointe and Minchin 2008, 2019) is a solver of coupled carbon and water flow in phloem and xylem respectively, following Münch Theory (Münch 1930). In both models, PiafMunch and CPlantBox, the topology of the plant is abstracted as a set of connected nodes in 3D space. On top of the topology, functional parameters such as axial resistance of xylem and phloem, maintenance, loading rate and unloading rate are assigned on each node or connection. From this information, PiafMunch simulates the advective transport of carbohydrates through the phloem within the whole structure and returns the amount of carbon (delivered by sieve-tube flow) available for unloading at any node. Water flow in both xylem and phloem follows the Hagen–Poiseuille's law. The hydraulic water potential gradient and pressure gradient drive both the xylem and phloem water flow, while only the phloem water flow with dissolved carbon is affected by the pressure generated by the osmotic gradients (Münch Hypothesis). There is water flow exchange between the xylem vessels and phloem vessels, which depends on the pressure and resistance between xylem and phloem, throughout the simulation. The carbon unloading is described as a first-order kinetic process in which the unloading rate is linearly dependent on the carbon concentration in the sieve tubes at each root tip. Excess carbon (unloaded carbon not used for the growth of the root tip) is considered to be exuded.

Here, we connected both models, such that, at each time step, the plant architecture is computed by CPlantBox, sent to PiafMunch, that in turn sends back to CPlantBox the amount of carbon available for growth at each root tip. The development of the structure in CPlantBox at the next time step is therefore constrained by the available carbon. The dynamic feedback loop between both models is illustrated in Fig. 2 and explained below.

2.2 Dynamic feedback between structures and functions

A Jupyter Notebook (Perkel 2018) was used as a mid-ware to control both CPlantBox (run under Windows Subsystem for Linux) and PiafMunch (run under Windows), see Section Code Availability. The Jupyter Notebook was used to initialize parameters and run simulations. A more detailed description of the method can be found in Supporting Information—S1.

2.2.1 Stage 1: initialization of architecture growth.

Most parameters of CPlantBox, such as organ radius, potential growth rate and potential topological structure of each plant are kept constant throughout the simulation. The actual root growth rate, which was a parameter in our previous study (Zhou *et al.* 2020), is now changed to a variable in this study. The actual growth rate varies depending on the carbon delivered to the root tip in this study. Although it is possible to generate some stochasticity by adding deviation to the parameters, in the results of this paper, we did not use any stochasticity except the random emergence of laterals, which will be shown in the results of *in silico* experiment 3.

2.2.2 Stage 2: Anatomy.

Similar to the initialization of CPlantBox, most parameters of PiafMunch are also kept constant throughout *in silico* experiments 1–3 except local phloem resistances, that are based on local anatomies (driven by changes in diameters). Phloem resistivity and sieve-tube radius of specific root types, maximum loading rate and maximum unloading rate of each source or sink are kept constant in each *in silico* experiment. Details about the estimation of the different parameters are given in Stage 5.

While the root xylem radial and axial resistances are computed based on their local segment age (Supporting Information—Fig. S2) (Doussan *et al.* 1998; Heymans *et al.* 2021), the sieve-tube axial resistances are assumed to be constant within root types and not age dependent. The phloem axial resistivities are calculated according to the Poiseuille law for water flow in a cylindrical tube, that is they are inversely proportional to the fourth power of the sieve-tube radius (Equation 1, see Supporting Information—S2 and Fig. S1).

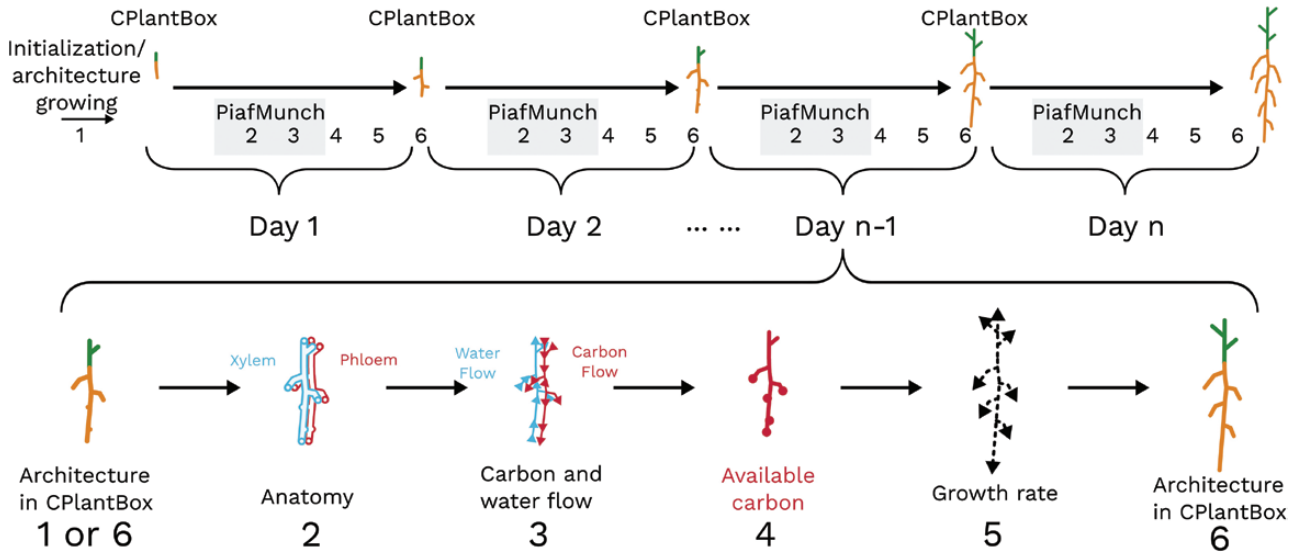

Figure 2. A simulation from Day n to Day $n + 1$ includes six stages. The Stage 1 of the simulation is 'initialization/architecture growing', which initials the plant in CPlantBox before Day 1. The Stage 1 only happens once per simulation run (once per treatment). During Day 1, a very tiny plant (the most left column in the upper row) is growing. For each following simulation day, the simulation runs from Stage 2 to Stage 6, to calculate the growth rate on each root tip. Details about the different stages can be found in the Section 2.2.

$$R_{\text{phloem -segment}} = \frac{R_{\text{single\_sieve-tube}}}{N_{\text{st\_cross}}} = \frac{8 \cdot \eta \cdot l_{\text{single\_sieve-tube}}}{\pi\left(\frac{d_{\text{single\_sieve-tube}}}{2}\right)^4 \cdot N_{\text{st\_cross}}} \quad (1)$$

In Equation 1, $R_{\text{phloem-segment}}$ (MPa h ml^{-1}) is the resistance of a phloem segment, $R_{\text{single\_sieve-tube}}$ (MPa h ml^{-1}) is the resistance of a single phloem sieve tube, $N_{\text{st\_cross}}$ (dimensionless) is the number of sieve tubes in a root cross section (dimensionless), η is the viscosity of the phloem sap, which is assumed to be constant as 1.7 (mPs···s), $l_{\text{single\_sieve-tube}}$ (cm) is the length of the root segment, $d_{\text{single\_sieve-tube}}$ (cm) is the diameter of a single sieve tube. We assume the phloem resistance caused by the sieve plate is also proportional to resistance caused by the change of the sieve-tube radius (see Supporting Information—Fig. S1).

2.2.3 Stage 3: carbon and water flow.

At Stage 3, PiafMunch takes the architecture and anatomy information generated in Stage 2, to simulate the carbon and water flow as explained in (Zhou *et al.* 2020). Although only carbon is studied in all the three *in silico* experiments, water is also simulated in PiafMunch. This is because xylem water flow is a prerequisite of the carbon flow, see (Minchin and Lacointe 2017) for details. At the end of Stage 3, the available carbon is allocated to the different plant segments.

2.2.4 Stage 4: available carbon.

Once the carbon is allocated to the different part of the plants (local segments), the amount of carbon available for growth needs to be computed, based on the local maintenance and growth demands.

The dry mass of each root segment is calculated by the following equation:

$$M_{\text{root}} = \rho_{\text{dry}} \times V_{\text{root}} = \rho_{\text{dry}} \times \pi \times \left(\frac{d_{\text{root}}}{2}\right)^2 \times L_{\text{root}} \quad (2)$$

In Equation 2, V_{root} (cm^3) is the volume of one root segment, d_{root} (cm) is the diameter of the root segment, L_{root} (cm) is the length of this root segment and ρ_{dry} (g cm^{-3}) is the dry mass density of root which is set to 0.1 (g cm^{-3}) according to (Drouet and Pagès 2003). The total carbon of a segment used for maintenance is set to zero.

In this stage, available carbon is calculated in the form of carbon satisfactory rate S_{carbon} (dimensionless, calculated from g g^{-1}), which is the available carbon to be divided by the carbon needed for reaching full potential growth rate. The available carbon is equal to the carbon budget of cell wall formation divided by the carbon flow reaching the growing tip. Carbon maintenance only depends on the length of the segment.

$$V_{\text{Growth}} = L_{\text{Growth}} \times \pi \times \left(\frac{d_{\text{Segment}}}{2}\right)^2 \quad (3)$$

Where V_{Growth} (cm^3) is the volume of the root segment, L_{Growth} (cm) is the length of the segment, d_{Segment} (cm) is the diameter of the segment.

$$M_{\text{Growth}} = V_{\text{Growth}} \times \rho_{\text{dry}} \quad (4)$$

Where M_{Growth} (g) is the root mass of the potential growth, V_{Growth} (cm^3) is the volume of the potential growth, ρ_{dry} (g cm^{-3}) is the dry mass density of the root.

$$C_{\text{Potential}} = K_{\text{Carbon\_content}} \times M_{\text{Growth}} \quad (5)$$

Where $C_{Potential}$ is the carbon content (g) used for potential growth, $K_{carbon\_content}$ (dimensionless g g^{-1}) is the carbon content percentage in the root mass.

$$C_{Available} = J_{Carbon} \times \Delta t \times K_{Molar\_mass\_of\_carbon} \quad (6)$$

Where $C_{Available}$ is the carbon available (g) for growth in the current segment. J_{Carbon} is the carbon inflow (mmol h^{-1}) of the current segment, $K_{Molar\_mass\_of\_carbon}$ is the molar mass constant of carbon, here is approximately 0.012 (g $mmol^{-1}$).

$$S_{Carbon} = \frac{C_{Available}}{C_{Potential}} \quad (7)$$

Where S_{Carbon} (dimensionless, calculated from g g^{-1}) is the carbon satisfaction rate for growth in the current segment. $C_{Available}$ (g) is the carbon available for growth in the current segment, $C_{Potential}$ (g) is the needed carbon for maximal potential growth rate. The maximal growth rate (potential growth rate) is prescribed in the parameter file of CPlantBox.

2.2.5 Stage 5: growth rate.

In CPlantBox, the available carbon limits the potential growth rate of individual roots via a carbon satisfactory rate S_{Carbon} calculated in Stage 4. The S_{Carbon} is calculated as the ratio between the carbon needed for the potential growth rate (as defined in the CPlantBox parameter set) and the local carbon availability, as defined by PiafMunch, at each time step. The actual growth rate is therefore calculated by multiplying the potential growth rate and the carbon satisfactory rate. Each individual root tip uses the corresponding actual growth rate, g_{actual} (cm day^{-1}), in the next time step. The calculation is based on the following equation,

$$g_{actual} = f(S_{carbon}) = \begin{cases} g_{potential} \cdot S_{carbon} & \text{if} \quad S_{carbon} < 1 \\ g_{potential} & \text{otherwise} \end{cases} \quad (8)$$

where S_{carbon} is the carbon satisfactory rate (dimensionless, calculated from g g^{-1}); $g_{potential}$ is the potential growth rate (cm day^{-1}).

2.2.6 Stage 6: new architecture in CPlantBox.

Unlike the initialization stage, which happens only once per simulation run, the root architecture grows at every time step. For simplicity, and to confine our study to the root system development, we assume that the shoot growth rate is not affected by carbon or water. However, the actual root growth rate is calculated for each root tip, depending on the potential growth rate (as defined in the parameter file, which is identical among each *sub-type*) and the available carbon (as defined by PiafMunch in the previous time step). The actual growth rate is therefore always equal or lower than the potential growth rate as it may be limited due to the local carbon availability.

2.3 Description of the *in silico* experiments

We designed three *in silico* experiments to test the hypothesis that local root anatomies influence the formation of the root system architecture. In each *in silico* experiment, three contrasted treatments were simulated for 15 days. In all treatments of each *in silico* experiment, all the structural and functional parameters are kept as constant as possible (shown in Supporting Information—S1). The simulated plant is a simple plant, with a single taproot bearing first-order lateral roots. The shoot growth and development is the same in all three *in silico* experiments (1–3) and not influenced by the carbon distribution within the plant. This is done to confine our study to the root system. An overview of the *in silico* experiments 1–3 is given below and summarized in Table 1.

2.3.1 In silico experiment 1: variations in tap root resistivity influence only the tap root growth.

In the first *in silico* experiment, we quantified the effect of taproot phloem resistivity changes on the carbon flow toward the root system and the consequence on the root system development. To do so, we only changed the taproot phloem resistivity between the plants of this *in silico* experiment. The resistivity of the taproot in the three plants are 50%, 100% and 200% respectively. The taproot resistivity variation in the *in silico* experiment 1 is much lower than the variation in the laterals of *in silico* experiment 2, because (i) this level of variation is enough to make a difference, (ii) high variation will make distinct incomparable root architecture. All three treatments are simulated from the same CPlantBox parameter file. Therefore, the potential architecture of the three plants are identical.

2.3.2 In silico experiment 2: variations in lateral sieve-tube radius influence the lateral root growth.

In the second *in silico* experiment, we quantified the effect of the heterogeneous resistivity in lateral roots (induced by the heterogeneity of sieve-tube radii) on the carbon flow toward the root system and the consequence on the root system development. In this *in silico* experiment, we changed the initial lateral root sieve-tube radius (i.e. constant throughout the *in silico* experiment) for the different treatments. The resistivity of the laterals in the three plants are 50%, 100% and 150% respectively.

2.3.3 In silico experiment 3: Non-uniform lateral sieve-tube radii influence non-uniformly lateral root growth.

In the third *in silico* experiment, we quantified the effect of the lateral root sieve-tube radius heterogeneity on the carbon flow toward the root system and the consequence on the root system development. In contrast with experiment 2, in this *in silico* experiment, three types of lateral roots with different sieve-tube radii are grown in random order on the taproot in each treatment. The aim of this third *in silico* experiment is to isolate potential pleiotropic effects of changes in carbon allocation.

3. RESULTS

3.1 Overview of the analysis pipeline

In this study, we wanted to observe and quantify the theoretical effect of (i) sieve-tube resistivity on the local carbon flow within the root system and (ii) the effect of the subsequent carbon (delivered by carbon flow) allocation on the root system growth. To achieve this goal, we used a novel combination of computational plant models.

First, we used the model CPlantBox (Zhou *et al.* 2020) to create a growing 3D plant structure (root and shoot), from a default user-defined parameter set. Second, we used a mechanistic model of phloem and xylem flow, PiafMunch (Lacointe and Minchin 2019), to solve the distribution of carbohydrates within the plant. Third, we created a dynamic feedback loop function between both models, such that the distribution of carbohydrates (in PiafMunch), at each time step, influences the formation of the plant architecture at the next time step (in CPlantBox). This allowed us to quantify the mutual effect between the distribution of carbohydrates and the establishment of the plant architecture.

The effect of the root phloem anatomy on the carbon distribution and root development was achieved via the modification of the phloem hydraulic conductivity (Zwieniecki *et al.* 2002; Jensen *et al.* 2012; Knoblauch *et al.* 2016; Holbrook and Knoblauch 2018). Different phloem hydraulic resistance in both the primary root (*in silico* experiment 1) and the lateral roots (*in silico* experiments 2 and 3) lead to a different final root length. We also quantified the induced changes on the root system growth and development. Details about the different parts of our analysis pipeline are given in the Section 2.

3.2 Phloem resistivities constrain the final length of primary and lateral roots

In the different simulations, we changed the phloem resistivity of the primary root or the phloem resistivities of the lateral roots. We observed a direct influence of such change on the final length of the affected roots (Fig. 3). As a general rule, when the phloem resistivity of a root increases, its final length decreases. This was observed for the primary roots (Fig. 3A and B) and for the lateral roots (Fig. 3C–F).

In Fig. 3E and F, we can also observe that the decrease in final root length is a consequence of a local change in root phloem resistivity and not a pleiotropic effect at the root system level. Indeed, when mixing roots with different phloem resistivities within a single root system (Fig. 3E), we can see that the final length is influenced by these resistivities alone, and not the resistivities of the neighbouring roots. Furthermore, if we compare Fig. 3D and F, we can see that lateral roots with the same tube radius have similar behaviours, irrespective of their neighbours or position on the primary root. A comparison between 11 treatments in the *in silico* experiment 3 and the linear regressions of *in silico* experiment 2 is shown in Supporting Information—Fig. S5.

3.3 Phloem resistivity constrains the growth duration of primary and lateral roots

In addition to the effect of the phloem (single sieve tube) resistivity on the final length of the roots, it seems to have a strong effect on the growth duration of individual roots (Fig. 4). In our model, the actual growth rate is indeed modulated by the amount of carbohydrates available at the root tip. If that amount is not enough to sustain the potential growth rate, as defined in the original parameter set, the growth rate is adjusted.

Again, for both the primary and the lateral roots, we observed that the changes in phloem resistivity impose strong constraints on the growth rate. For the tap roots, the growth is identical for the first 7 days, independently of the phloem resistivity (Fig. 4A). After the 7th day, the root with the largest resistivity decreases its growth, then stops after the 15th day completely. The same can be observed after 7 days for the roots with 100% and 50% single sieve-tube resistivity, respectively.

For the lateral roots, the picture is less clear, as many roots are influenced at the same time. However, the same dynamic can be observed as for the primary root. Indeed, the duration of the growth period seems to be directly linked to the hydraulic resistivity of the phloem (Fig. 4B). As the phloem resistivity of individual roots increases, the growth period of these roots shortens.

Newly formed leaves act as additional carbon sources as shown in Fig. 4C. The increased carbon loading leads to an increase of the growth rates (e.g. on Day 9 and Day 12 in Fig. 4A). Although the same amount of new carbon was loaded into the phloem conduits on Day 9 and Day 12, the growth rate increment of the three treatments are different. The growth rates of the low-resistance treatment is equal for both days while the growth rate of two higher resistance treatments are lower on Day 12 than the growth rate of on Day 9.

The lateral growth rate changing trends also differed between the three treatments of *in silico* experiment 2 as shown in Fig. 4B. The growth rate of high resistance lateral is lower, which is similar to *in silico* experiment 1. However, we observe less fluctuation on Day 9 and Day 12.

3.4 Local phloem resistivities influence carbon allocation between the root and the shoot

The observed changes in growth can be linked to changes in the carbohydrate flow within the root systems. In the different simulations, the total carbon production was equal across the *in silico* experiments 1–3 (same loading rate of carbohydrates in the phloem at the shoot level) (Fig. 5A). However, the carbon allocation between the root sieve tubes (Fig. 5C) and the shoot sieve tubes (Fig. 5B) was different in the three treatments. We can indeed observe that in larger primary root resistance result in sieve-tube carbon content is lower in the root and higher in the shoot. The divergence of the sieve tube carbon content indicates the root system hydraulic profile, as more carbon needs to stay in the shoot sieve tube to overcome the root phloem hydraulic resistance. The total amount of carbon in Fig. 5A is equal to the sum of Fig. 5B and C. It is very interesting to see that the carbon content in sieve tubes reached equilibrium by distributing carbon content between the shoots (sources) and roots (sinks).

These allocation patterns are not predefined in the model, but the output of the mechanistic model which describes the carbon flow within the system. The changes in allocation are therefore a direct consequence of the altered phloem resistivities (additional Figures in Supporting Information—S2, Fig. S3-4 and additional simulation for 30 days in Supporting Information—S3).

4. DISCUSSION

4.1 Phloem resistance creates a sink limitation to carbohydrate flow

In our simulations, we could observe a strong limitation to the carbon flow in the system due to changes in the conductivities along the carbon pathways (and not directly due to changes in local carbon sink strength). As the carbon loading at the leaf level

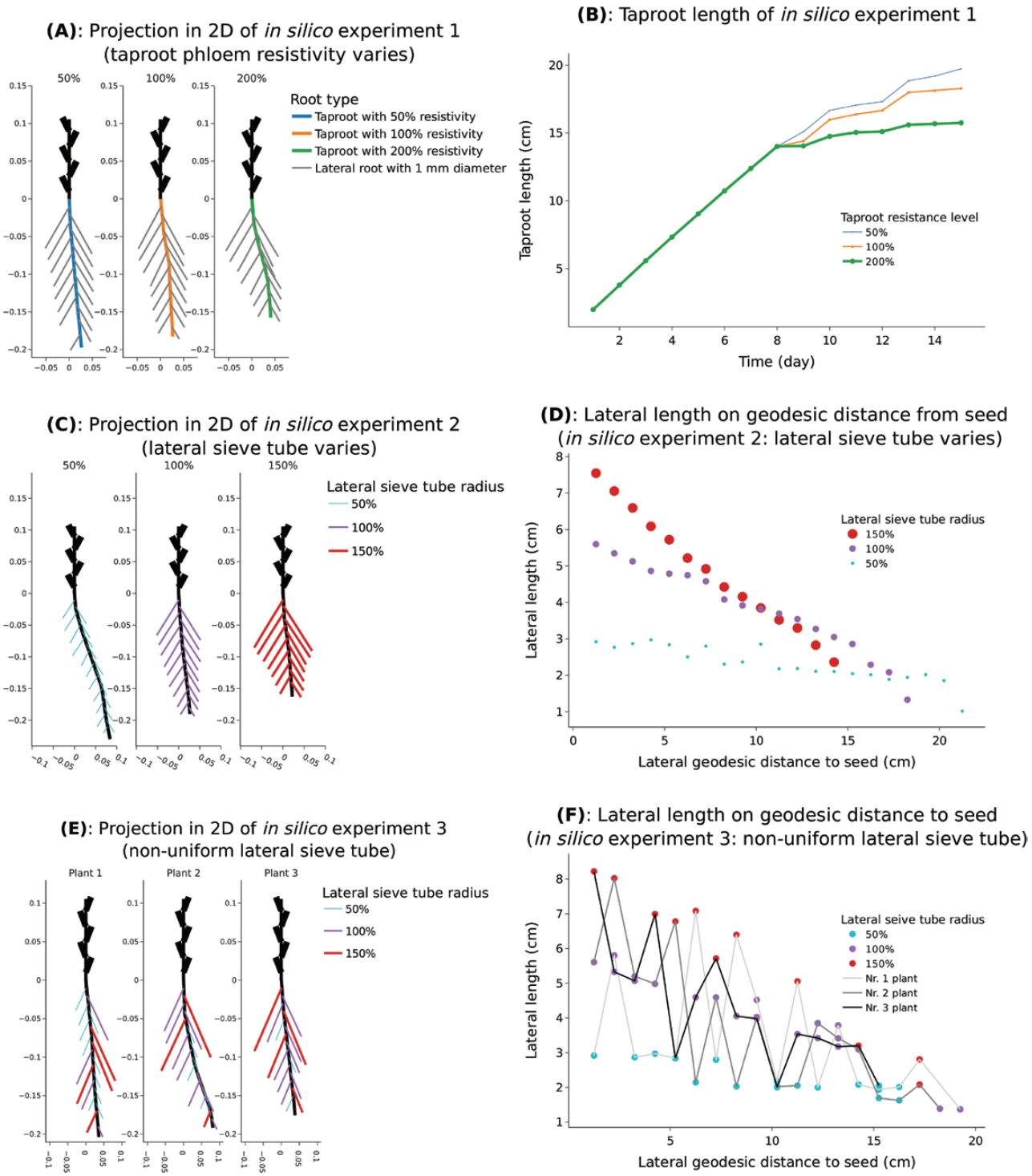

Figure 3. Growth patterns of *in silico* experiment 1–3 in two-dimensional projections and length charts. A: 2D projection of *in silico* experiment 1 (tap root sieve-tube varies); B: Roots with a higher resistance (thick lower line) grow for a shorter time compared to roots with a low resistance (thin upper line). C: 2D projection of experiment 2 (lateral sieve-tube varies). D: Length of the lateral roots for the different scenarios, as a function of their insertion geodesic distance from the seed. E: 2D projection of the root systems from *in silico* experiment 3 (non-uniform laterals with different sieve-tube radius). F: Length of the lateral roots for the different scenarios, as a function of their insertion geodesic distance from the seed. Scatter points are connected into lines to represent different plants.

was set at a constant value in all simulations, the total amount of carbohydrates injected into the system was constant for each leaf (and therefore increasing during the simulation as new leaves were produced Fig. 4C). However, the distribution (allocation) of the carbohydrates within the plant was strongly influenced by total root phloem resistances (Fig. 3D and F and see Supporting Information—Fig. S5). In our simulations, the phloem anatomy was therefore directly linked to a sink limitation of carbon flow within the plant. As the root phloem resistance along the path of carbohydrates becomes too high, the flow decreases to a stop,

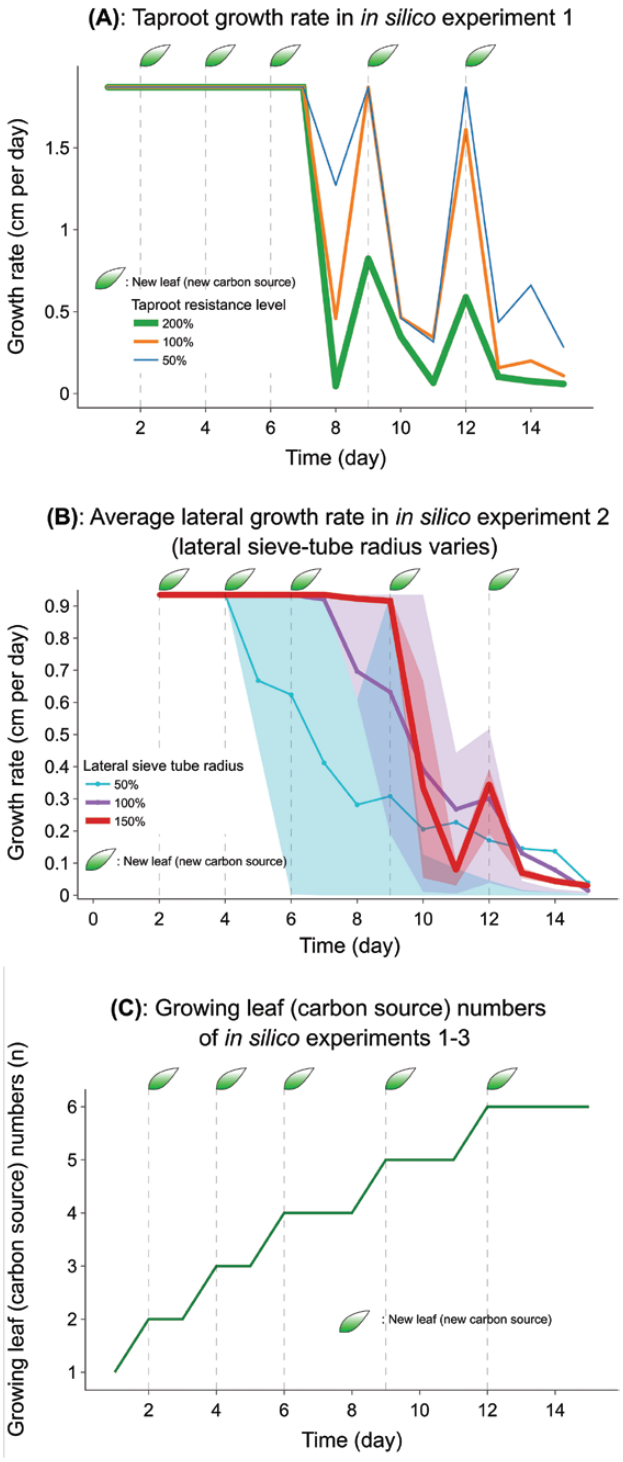

Figure 4. Daily root growth rate is affected by both the phloem resistivity and carbon source input, while the phloem resistivity is the deciding factor of final root length. A: The increase of tap root growth rate on Day 12 is caused by a newly growing leaf, which loads more carbon into the phloem; B: Average (colored lines) and quantile (25% to 75% in colour area) of the laterals' growth rates in the *in silico* experiment 2 show variability among the root growth rate of the three plants; C: Five plant leaves are grown consecutively on Day 2, 4, 6, 9 and 12.

preventing the resources, which are needed for individual root growth, to reach the root apexes. It is worth noting that, in our simulations, the limitation is not at the sink itself (the potential demand for carbon was identical in all simulations), but on the path of carbon leading to that sink. If that path is limiting the flow, it becomes impossible to push carbohydrates along the roots, no matter how strong the local demand at the apexes is. This brings a new perspective to previous published studies that have shown a strong effect of local root tip demand on the global architecture, but did not take the resistance along the phloem vasculature explicitly into account (Pagès *et al.* 2020).

From a breeding perspective, this indicates that the phloem resistance in the roots can be a strong restriction to root/shoot allocation manipulation. If we aim at creating larger root systems, either to access more resources (Lobet *et al.* 2012; Lynch 2013; Lobet, Couvreur, *et al.* 2014) or to store mode carbon within the soil (Bidel *et al.* 2000; Dilkes *et al.* 2004), it is critical to take this sink limitation into account.

4.2 Phloem anatomy as a driver of root architecture

Our simulation results indicate that, in theory, local phloem resistance can have a strong influence on the growth and development of single roots and therefore influence the shape and function of the root system as a whole. The effects observed in this study are limited to small plant architectures but are expected to become larger as the plant grows. Small effects observed at the beginning of the growing period will accumulate during the root system development, leading to very distinct developmental trajectories (see Supporting Information—Fig. S6).

This opens up interesting perspectives in root research. It means that some specific phloem developmental traits, such as to locally increase or decrease its resistivity, has the potential to manipulate the growth and development of specific root types and to shape the root system architecture as a whole.

From a root modelling perspective, our results suggest that the final root length of specific roots could be seen as output of the model (additional simulation for 30 days in Supporting Information—S3), rather than inputs, as it is the case with most current root models (Pagès *et al.* 2004, 2014; Postma *et al.* 2017; Schnepf *et al.* 2018). However, the modelling approach described here is likely to be too demanding in terms of computing resources, making it impractical for large-scale modelling studies. A tighter integration between the different models (here CPlantBox and PiafMunch) or the use of upscaling methods could help to incorporate these mechanistic processes into larger scale models.

4.3 Phloem anatomical variance explains uneven development between roots with different diameters

Many studies have established links between root diameter and function. For instance, root diameter has been shown to be linked to specific root length and mycorrhizal colonization (Ma *et al.* 2018), foraging capacity (Colombi *et al.* 2017) or the root capacity to uptake water (Heymans *et al.* 2020). Root diameter has also been linked to root developmental properties such as growth rate (Pagès and Picon-Cochard 2014), branching density (Pagès 2016) or root system architecture as a whole (Pagès and Kervella 2018). These links have been shown to hold true between species, but also within single plants. Although the ρ_{dry} is set to a constant parameter in the simulation, the output

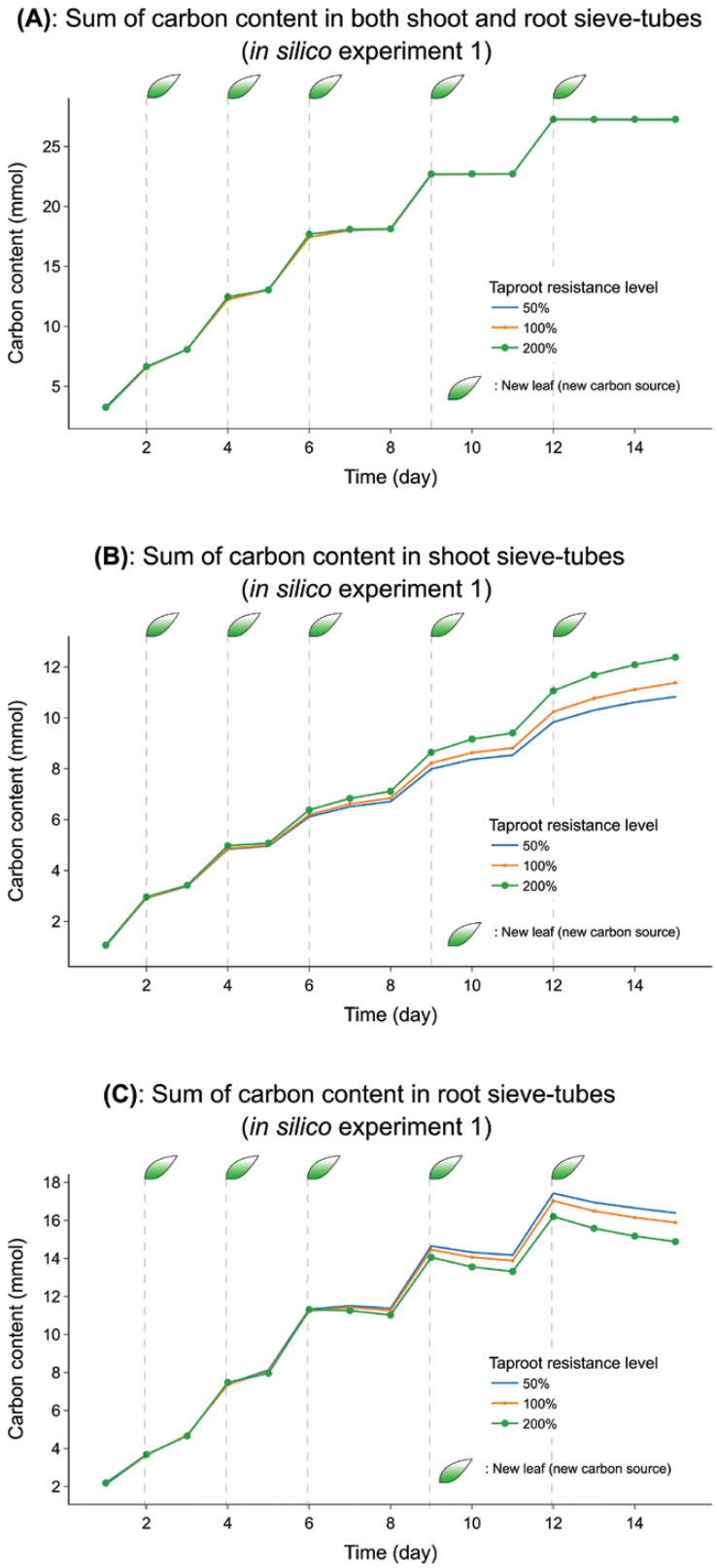

Figure 5. Comparison among the sums of sieve-tube content (but not the accumulated carbon distribution) of whole plants, shoots and roots in the *in silico* experiment 1. A: After the 8th day, the sum of all sieve-tube solute carbon content in the whole plant is the same between the three treatments. The slight difference, which is caused by the newly growing leaves (explained in Supplementary Information), mainly showed up during the first 8 days. B: In the shoot, leaves are growing, which in turn increase the sieve-tube carbon content. C: In the root, the sums of sieve-tube carbon content in the three plants are similar during the first 6 days, because the root sizes are similar. Later on, the root with larger resistivity grows less, in turn the plant with high phloem resistance has smaller root size and contains less carbon content.

roots are actually equipped with diverse root-specific length (see Supporting Information—Fig. S6). This result also aligned with the previous publications (Freschet *et al.* 2015; Rose 2017; Rose and Lobet 2019). Recent studies have quantified the growth and development of several root types growing on the same primary roots (Passot *et al.* 2016, 2018; Muller *et al.* 2019). Recently, a clear connection between phloem diameter and growth was shown by (Tang *et al.* 2022). These different root types have been shown to have contrasting anatomy, growth rate and final length, leading to highly heterogeneous root system architectures, even within homogeneous conditions.

We were able to qualitatively reproduce various distinct developmental dynamics (Clerx *et al.* 2020; Lupi *et al.* 2010; Tang *et al.* 2022) (differences in growth rate and final length) by changing only the root phloem resistivities. As phloem resistivity is, to some extent, linked to the root diameter (as the diameter increases the number of phloem poles increases as well), our simulation results could explain some of the differences observed between roots of different diameters (Passot *et al.* 2016, 2018; Muller *et al.* 2019).

4.4 Current limitations of the model

By design, our *in silico* experiments focussed on the growth and development of the root system. For simplification purposes, we did not explore the effect of local resistance changes in the shoot. We also did not include feedback mechanisms between the carbon allocation and shoot functional features such as leaf area, leaf thickness or photosynthetic efficiency, that all have been shown to respond to changes in allocation patterns. On the root system side, root density (ρ_{dry}), which directly affects the root structural growth, is set to a fixed value. Again, changes in tissue density have been shown experimentally to vary with carbon allocation (Freschet *et al.* 2015), which might modulate our theoretical results. However, we feel these additional feedback loops within the model would not change the interpretation of our main results.

5. CONCLUSION

In this study, we have used a computational pipeline to explore the interplay between local phloem hydraulic properties and the global root system development. We have shown that a local decrease in the phloem conductivity can lead to shorter roots, with a slower growth rate and shorter growth duration. We have also shown that this change in architecture was not due to a pleiotropic effect at the plant level, but mainly a local effect of the phloem properties.

Our results are well in line with experimental results that have studied the link between root diameter, length and growth. They provide a simple mechanistic explanation to the variety of root types observed experimentally and provide an alternative explanation to the effect of root tip sinks alone.

Finally, from a modelling point of view, our results provide a first example where the features of single roots within the root system (such as their growth rate and final root length) are not prescribed a priori but are an emergent property of the system. This opens the way to move plastic representation of the root system within computational models.

SUPPORTING INFORMATION

The following additional information is available in the online version of this article –

Each of the three directories ('Experiment1', 'Experiment2' and 'Experiment3') contains all the input and output data of the *in silico* experiment 1, *in silico* experiment 2 and *in silico* experiment, 3 respectively.

-The 'ini' input files are used for each plant's carbon and water flow simulation.

-The 'txt' output files are the result of the carbon and water flow simulation.

-The 'csv' file contains the information of the figures and the 'vtp' file can be used for animation.

ACKNOWLEDGEMENTS

This research was supported by Agrosphäre, IBG-3 Forschungszentrum Jülich. We thank our colleagues from UMR PIAF who provided insight and expertise that greatly assisted the research, although they may not agree with all of the interpretations of this paper.

CONTRIBUTIONS BY THE AUTHORS

Writing—original draft: X.-R.Z., G.L.; writing—review and editing: J.V., H.V., G.L., X.-R.Z.; conceptualization: G.L., A.S., H.V., J.V., X.-R.Z.; software: X.-R.Z., D.L., A.S., G.L.; visualization: X.-R.Z., G.L., J.V.

CONFLICT OF INTEREST STATEMENT

No conflict of interest.

DATA AVAILABILITY

Data is open accessible at https://doi.org/10.5281/zenodo.8318386 and github at https://github.com/Plant-Root-Soil-Interactions-Modelling/CPlantBox/tree/zhou2022/tutorial/jupyter/zhou_2022.

CODE AVAILABILITY

The code used in this paper is available here https://doi.org/10.5281/zenodo.8318386 and here https://github.com/Plant-Root-Soil-Interactions-Modelling/CPlantBox/tree/zhou2022.

REFERENCES

Ahmed M, Aslam MA, Fayyaz-ul-Hassan Hayat R, Nasim W, Akmal M, Mubeen M, Hussain S, Ahmad S. 2022. Nutrient dynamics and the role of modeling In: Jatoi WN, Mubeen M, Ahmad A, Cheema MA, Lin Z, Hashmi MZ, eds. *Building Climate Resilience in Agriculture: Theory, Practice and Future Perspective*. Cham: Springer International Publishing, 297–316.

Bidel L, Pages L, Riviere LM, Pelloux G, Lorendeau JY. 2000. MassFlowDyn I: a carbon transport and partitioning model for root system architecture. *Annals of Botany* 85:869–886.

Clerx LE, Rockwell FE, Savage JA, Holbrook NM. 2020. Ontogenetic scaling of phloem sieve tube anatomy and hydraulic resistance with tree height in *Quercus rubra*. *American Journal of Botany* 107:852–863.
Colombi T, Kirchgessner N, Walter A, Keller T. 2017. Root tip shape governs root elongation rate under increased soil strength. *Plant Physiology* 174:2289–2301.
De Bauw P, Mai TH, Schnepf A, Merckx R, Smolders E, Vanderborght J. 2020. A functional–structural model of upland rice root systems reveals the importance of laterals and growing root tips for phosphate uptake from wet and dry soils. *Annals of Botany* 126:789–806.
de Vries J, Evers JB, Kuyper TW, van Ruijven J, Mommer L. 2021. Mycorrhizal associations change root functionality: a 3D modelling study on competitive interactions between plants for light and nutrients. *The New Phytologist* 231:1171–1182.
Delory BM, Baudson C, Brostaux Y, Lobet G, du Jardin P, Pagès L, Delaplace P. 2016. archiDART: an R package for the automated computation of plant root architectural traits. *Plant and Soil* 398:351–365.
Dilkes NB, Jones DL, Farrar J. 2004. Temporal dynamics of carbon partitioning and rhizodeposition in wheat. *Plant Physiology* 134:706–715.
Doussan C, Page LC, Vercambreå G. 1998. Modelling of the hydraulic architecture of root systems: an integrated approach to water absorption–model description. *Annals of Botany* 81:213–223.
Drouet J-L, Pagès L. 2003. GRAAL: a model of GRowth, Architecture and carbon ALlocation during the vegetative phase of the whole maize plant: model description and parameterisation. *Ecological Modelling* 165:147–173.
Freschet GT, Swart EM, Cornelissen JHC. 2015. Integrated plant phenotypic responses to contrasting above- and below-ground resources: key roles of specific leaf area and root mass fraction. *The New Phytologist* 206:1247–1260.
García-Cervigón AI, Fajardo A, Caetano-Sánchez C, Camarero JJ, Olano JM. 2020. Xylem anatomy needs to change, so that conductivity can stay the same: xylem adjustments across elevation and latitude in *Nothofagus pumilio*. *Annals of Botany* 125:1101–1112.
Heymans A, Couvreur V, LaRue T, Paez-Garcia A, Lobet G. 2020. GRANAR, a computational tool to better understand the functional importance of monocotyledon root anatomy. *Plant Physiology* 182:707–720.
Heymans A, Couvreur V, Lobet G. 2021. Combining cross-section images and modeling tools to create high-resolution root system hydraulic atlases in *Zea mays*. *Plant Direct* 5:e334.
Holbrook NM, Knoblauch M. 2018. Editorial overview: physiology and metabolism: phloem: a supracellular highway for the transport of sugars, signals, and pathogens. *Current Opinion in Plant Biology* 43:iii–vii.
Jensen KH, Mullendore DL, Holbrook NM, Bohr T, Knoblauch M, Bruus H. 2012. Modeling the hydrodynamics of phloem sieve plates. *Frontiers in Plant Science* 3:151.
Kahlen K, Chen T-W. 2015. Predicting plant performance under simultaneously changing environmental conditions—the interplay between temperature, light, and internode growth. *Frontiers in Plant Science* 6:1130.
Knoblauch M, Knoblauch J, Mullendore DL, Savage JA, Babst BA, Beecher SD, Dodgen AC, Jensen KH, Holbrook NM. 2016. Testing the Münch hypothesis of long distance phloem transport in plants. *eLife* 5:e15341.
Lacointe A, Minchin PEH. 2008. Modelling phloem and xylem transport within a complex architecture. *Functional Plant Biology* 35:772–780.
Lacointe A, Minchin PEH. 2019. A mechanistic model to predict distribution of carbon among multiple sinks. *Methods in Molecular Biology* 2014:371–386.
Landl M, Haupenthal A, Leitner D, Kroener E, Vetterlein D, Bol R, Vereecken H, Vanderborght J, Schnepf A. 2021. Simulating rhizodeposition patterns around growing and exuding root systems. *in silico Plants* 3:diab–028. doi:10.1093/insilicoplants/diab028
Leitner D, Klepsch S, Bodner G, Schnepf A. 2010. A dynamic root system growth model based on L-Systems. *Plant and Soil* 332:177–192.
Lobet G, Couvreur V, Meunier F, Javaux M, Draye X. 2014. Plant water uptake in drying soils. *Plant Physiology* 164:1619–1627.
Lobet G, Pagès L, Draye X. 2012. A modeling approach to determine the contribution of plant hydraulic conductivities on the water uptake dynamics in the soil-plant-atmosphere system In: 2012 IEEE 4th International Symposium on Plant Growth Modeling, Simulation, Visualization and Applications. 235–241.
Lobet G, Pagès L, Draye X. 2014. A modeling approach to determine the importance of dynamic regulation of plant hydraulic conductivities on the water uptake dynamics in the soil-plant-atmosphere system. *Ecological Modelling* 290:65–75.
Lupi C, Morin H, Deslauriers A, Rossi S. 2010. Xylem phenology and wood production: resolving the chicken-or-egg dilemma. *Plant, Cell & Environment* 33:1721–1730.
Lynch JP. 2013. Steep, cheap and deep: an ideotype to optimize water and N acquisition by maize root systems. *Annals of Botany* 112:347–357.
Ma Z, Guo D, Xu X, Lu M, Bardgett RD, Eissenstat DM, McCormack ML, Hedin LO. 2018. Evolutionary history resolves global organization of root functional traits. *Nature* 555:94–97.
Minchin PEH, Lacointe A. 2017. Consequences of phloem pathway unloading/reloading on equilibrium flows between source and sink: a modelling approach. *Functional Plant Biology* 44:507–514.
Morandage S, Vanderborght J, Zörner M, Cai G, Leitner D, Vereecken H, Schnepf A. 2021. Root architecture development in stony soils. *Vadose Zone Journal* 20:e–20133. doi:10.1002/vzj2.20133
Muller B, Guédon Y, Passot S, Lobet G, Nacry P, Pagès L, Wissuwa M, Draye X. 2019. Lateral Roots: Random Diversity in Adversity. *Trends in Plant Science* 24:810–825.
Münch E. 1930. *Stoffbewegungen in der Pflanze*. Jena, Germany: Gustav Fischer.
Pagès L. 2016. Branching patterns of root systems: comparison of monocotyledonous and dicotyledonous species. *Annals of Botany* 118:1337–1346.
Pagès L, Bécel C, Boukcim H, Moreau D, Nguyen C, Voisin A-S. 2014. Calibration and evaluation of ArchiSimple, a simple model of root system architecture. *Ecological Modelling* 290:76–84.
Pagès L, Bernert M, Pagès G. 2020. Modelling time variations of root diameter and elongation rate as related to assimilate supply and demand. *Journal of Experimental Botany* 71:3524–3534.
Pagès L, Kervella J. 2018. Seeking stable traits to characterize the root system architecture. Study on 60 species located at two sites in natura. *Annals of Botany* 122:107–115.
Pagès L, Picon-Cochard C. 2014. Modelling the root system architecture of Poaceae. Can we simulate integrated traits from morphological parameters of growth and branching? *The New Phytologist* 204:149–158.
Pagès L, Vercambre G, Drouet J-L, Lecompte F, Collet C, Le Bot J. 2004. Root Typ: a generic model to depict and analyse the root system architecture. *Plant and Soil* 258:103–119.
Passot S, Gnacko F, Moukouanga D, Lucas M, Guyomarc'h S, Ortega BM, Atkinson JA, Belko MN, Bennett MJ, Gantet P, Wells DM, Guédon Y, Vigouroux Y, Verdeil J-L, Muller B, Laplaze L. 2016. Characterization of pearl millet root architecture and anatomy reveals three types of lateral roots. *Frontiers in Plant Science* 7:829.
Passot S, Moreno-Ortega B, Moukouanga D, Balsera C, Guyomarc'h S, Lucas M, Lobet G, Laplaze L, Muller B, Guédon Y. 2018. A new phenotyping pipeline reveals three types of lateral roots and a random branching pattern in two cereals. *Plant Physiology* 177:896–910.
Perkel JM. 2018. Why Jupyter is data scientists' computational notebook of choice. *Nature* 563:145–146.
Postma JA, Kuppe C, Owen MR, Mellor N, Griffiths M, Bennett MJ, Lynch JP, Watt M. 2017. OpenSimRoot: widening the scope and application of root architectural models. *The New Phytologist* 215:1274–1286.
Rose L. 2017. Pitfalls in root trait calculations: how ignoring diameter heterogeneity can lead to overestimation of functional traits. *Frontiers in Plant Science* 8:898.
Rose L, Lobet G. 2019. Accuracy of image analysis tools for functional root traits: a comment on Delory *et al.* (2017). *Methods in Ecology and Evolution/British Ecological Society* 10:702–711.
Schnepf A, Leitner D, Landl M, Lobet G, Mai TH, Morandage S, Sheng C, Zörner M, Vanderborght J, Vereecken H. 2018. CRootBox: a

structural–functional modelling framework for root systems. *Annals of Botany* 121:1033–1053.

Sharp RE, Poroyko V, Hejlek LG, Spollen WG, Springer GK, Bohnert HJ, Nguyen HT. 2004. Root growth maintenance during water deficits: physiology to functional genomics. *Journal of Experimental Botany* 55:2343–2351.

Tang Y, Yin S, Pace MR, Gerolamo CS, Nogueira A, Zuntini AR, Lohmann LG, Plath M, Liesche J. 2022. Diameters of phloem sieve elements can predict stem growth rates of woody plants. *Tree Physiology* 42:1560–1569.

Uys L, Hofmeyr J-HS, Rohwer JM. 2021. Coupling kinetic models and advection–diffusion equations. 1. Framework development and application to sucrose translocation and metabolism in sugarcane. *in silico Plants* 3:diab–013. doi:10.1093/insilicoplants/diab013

Zhong M, Castro-Díez P, Puyravaud J-P, Sterck FJ, Cornelissen JHC. 2019. Convergent xylem widening among organs across diverse woody seedlings. *The New Phytologist* 222:1873–1882.

Zhou X-R, Schnepf A, Vanderborght J, Leitner D, Lacointe A, Vereecken H, Lobet G. 2020. CPlantBox, a whole-plant modelling framework for the simulation of water- and carbon-related processes. *in silico Plants* 2:diaa–001. doi:10.1093/insilicoplants/diaa001

Zwieniecki MA, Thompson MV, Holbrook NM. 2002. understanding the hydraulics of porous pipes: tradeoffs between water uptake and root length utilization. *Journal of Plant Growth Regulation* 21:315–323.